How to cite: *Angew. Chem. Int. Ed.* **2023,** *62,* e202219091
International Edition: doi.org/10.1002/anie.202219091
German Edition: doi.org/10.1002/ange.202219091

Polycycles

Modular Synthesis of Structurally Diverse Azulene-Embedded Polycyclic Aromatic Hydrocarbons by Knoevenagel-Type Condensation

Renxiang Liu[+], Yubin Fu[+], Fupeng Wu, Fupin Liu, Jin-Jiang Zhang, Lin Yang, Alexey A. Popov, Ji Ma, and Xinliang Feng**

Abstract: The research interest in azulene-embedded polycyclic aromatic hydrocarbons (PAHs) has significantly increased recently, but the lack of efficient synthetic strategies impedes the investigation of their structure-property relationships and further opto-electronic applications. Here we report a modular synthetic strategy towards diverse azulene-embedded PAHs by a tandem Suzuki coupling and base-promoted Knoevenagel-type condensation with good yields and great structural versatility, including non-alternant thiophene-rich PAHs, butterfly- or Z-shaped PAHs bearing two azulene units, and the first example of a two-azulene-embedded double [5]helicene. The structural topology, aromaticity and photophysical properties were investigated by NMR, X-ray crystallography analysis and UV/Vis absorption spectroscopy assisted by DFT calculations. This strategy provides a new platform for rapidly synthesizing unexplored non-alternant PAHs or even graphene nanoribbons with multiple azulene units.

Introduction

Non-benzenoid non-alternant polycyclic aromatic hydrocarbons (PAHs) have gained considerable interdisciplinary attention in the past decade due to their special chemical reactivity, intriguing optoelectronic properties, and potential applications in organic electronics.[1] In particular, embedding an azulene unit, composed of a fused pentagon-heptagon (5–7 membered rings) pair, into π-extended PAHs has been intensively studied in recent years because it can modulate the electronic structures, molecular orbital characteristics, and geometries of the original alternant π-systems, leading to unprecedented chemical and physical properties, such as a narrow energy gap, abnormal anti-Kasha behavior, and significant open-shell character.[2] The classical methods to construct an azulene unit, such as Ziegler-Hafner's azulene synthesis from pyrylium salts,[3] Nozoe's synthesis from troponoids,[4] [8+2] cycloaddition of 2*H*-cyclohepta-[b]furan-2-ones with enamines,[5] and [6+4] cycloaddition of fulvenes,[6] have been widely used for preparing azulene extended derivatives with different functionalities. However, these approaches are difficult to be applied to construct large azulene-embedded PAHs due to the low reactivity and difficult access to the corresponding benzo-fused precursors.[3c] In addition to commencing the synthesis of these fascinating molecules from the parent azulene,[7] a surge of methods have been recently developed by us and others to in situ construct azulene subunits in the large π-systems either by on-surface synthesis[8] or by in-solution chemistry (Figure 1a), such as the Scholl-type cyclization,[9a–c] intramolecular Friedel-Craft reaction followed by aromatization,[10] alkyne annulation,[11] Pd-catalyzed [5+2] annulation[12] and photo-induced cyclization,[13] etc. Despite significant recent progress, the above transformations usually require multi-step synthesis of the specific precursors, and some products result from unpredicted rearrangement[9a,c] or insertion reactions.[11d,e] For example, the most commonly used Scholl reaction[14] under acidic conditions with 2,3-dichloro-5,6-dicyano-1,4-benzoquinone (DDQ)/acid or $FeCl_3$ to prepare non-alternant PAHs is sometimes difficult to be predicted,[9a,c] and is not a controllable tool for the construction of acid-sensitive pentagon-heptagon system.[15] Therefore, the development of a relatively simple and broadly applicable synthetic strategy toward structurally diverse azulene-embedded PAHs is highly desirable.

Recently, the Knoevenagel-type condensation reaction has been successfully utilized as a powerful tool to construct C=C bonds in alternant or non-alternant π-extended PAHs,[16] polyacene-type graphene nanoribbons[17] and even

[*] R. Liu,[+] Dr. Y. Fu,[+] F. Wu, Dr. J.-J. Zhang, L. Yang, Dr. J. Ma, Prof. Dr. X. Feng
Center for Advancing Electronics Dresden (cfaed) & Faculty of Chemistry and Food Chemistry, Technische Universität Dresden
01062 Dresden (Germany)
E-mail: ji.ma@tu-dresden.de
xinliang.feng@tu-dresden.de
Dr. F. Liu, Dr. A. A. Popov
Leibniz Institute for Solid State and Materials Research
Helmholtzstr. 20, 01069 Dresden (Germany)
Dr. J. Ma, Prof. Dr. X. Feng
Max Planck Institute of Microstructure Physics
Weinberg 2, 06120 Halle (Germany)
[+] These authors contributed equally to this work.

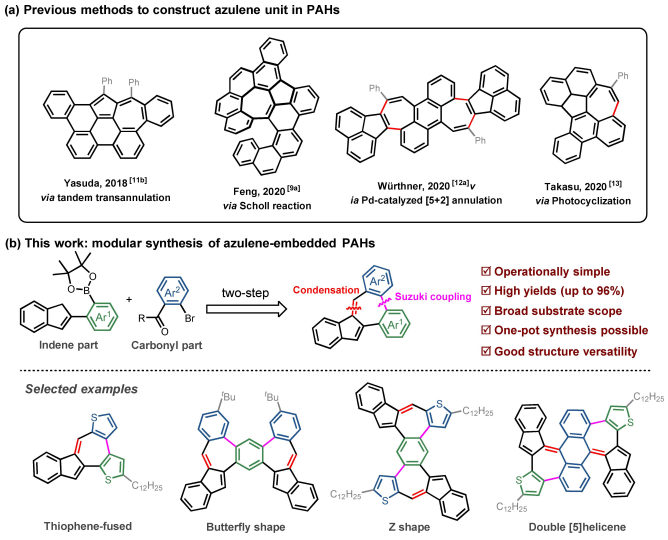

Figure 1. a) Representative known methods for the synthesis of azulene-embedded PAHs; b) Modular and efficient synthesis of azulene-embedded PAHs in this work.

vinylene-linked 2D conjugated polymers.[18] For example, Mastalerz et al. reported the construction of diarenoperylenes through intramolecular condensation reaction in 2016 and later extended this strategy towards the synthesis of benzo-fused perylene oligomers.[16a,c] In 2021, Scherf et al. also succeeded in the synthesis of a flexible graphene nanoribbon comprising a polyacene skeleton via a base-mediated condensation approach from a suitably functionalized polymer precursor.[17] Inspired by the high efficiency and flexible reaction conditions of Knoevenagel-type condensation, we envisioned that this transformation would be viable for further exploration of the in situ construction of the pentagon-heptagon pair (or azulene unit) in π-conjugated carbon framework, instead of the common hexagon-hexagon pair. To realize our hypothesis, we designed and synthesized a class of novel azulene-embedded PAHs with varied structures (**1a**–**1r**, 18 examples), including the benzene-, furan- or thiophene-condensed PAHs, butterfly- and Z-shaped large non-alternant PAHs, and a two-azulene-embedded double [5]helicene (Figure 1b), through a general two-step sequence: a Suzuki coupling of the indene unit with a carbonyl moiety, followed by a Knoevenagel-type condensation reaction as the final cyclization step. The feasible condensation step features good yields (up to 96 %) and great functional group tolerance since the two different aryl parts of substrates (Ar^1 and Ar^2) could be modified by diverse motifs and substituents. It is worth mentioning that the in situ condensation to afford azulene-embedded PAHs directly could also be realized from the biaryl precursor by increasing the amount of base in the Suzuki coupling reaction step, as exemplified by thiophene-fused product **1m**. The molecular geometric structures of representative examples containing one azulene (**1k**) or two azulene units (**1p**, **1q**) were unequivocally identified by single-crystal X-ray diffraction. Their aromaticity, electronic structures, and optical properties were fully investigated based on bond analysis, nucleus-independent chemical shifts (NICS), anisotropy of the induced current density (ACID), and the UV/Vis absorption spectroscopy and cyclic voltammetry.

Results and Discussion

We commenced our study on the base-promoted Knoevenagel-type intramolecular condensation reaction of rationally designed molecular precursor 5-(*tert*-butyl)-2′-(1*H*-inden-2-yl)-[1,1′-biphenyl]-2-carbaldehyde (**2a**) containing the indene unit (connect to Ar^1 apart) and carbonyl unit (in Ar^2 part). Remarkably, the addition of a strong base (*t*-BuOK) in the reaction system smoothly proceeded to furnish the desired 6-(*tert*-butyl)tribenzo[*a*,*e*,*g*]azulene (**1a**) with a high yield of 83 % (Table 1). To examine the applicability of this strategy, a series of structurally diverse precursors (**2b**–**2m**) with different Ar^1 and Ar^2 parts were synthesized with a

Table 1: Synthesis of non-alternant PAHs containing one azulene unit.[a]

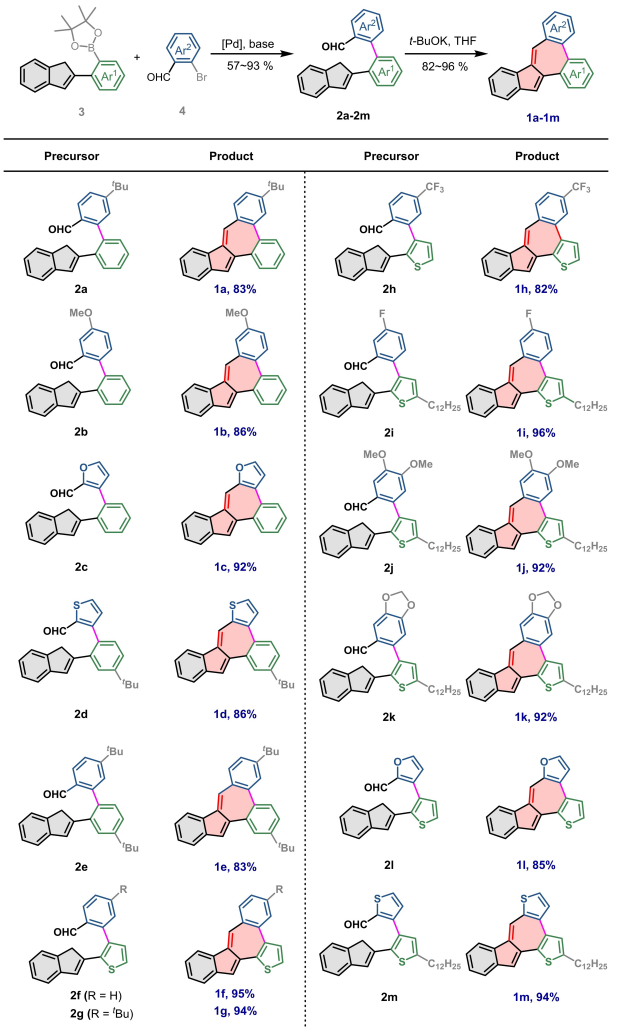

[a] Reaction conditions for **1a**–**1e**: **2** (1.0 equiv), *t*-BuOK (2.5 equiv) at r.t. for 30 min; reaction conditions for **1f**–**1m**: **2** (1.0 equiv), *t*-BuOK (2.5 equiv) at 0 °C for 20 min.

high yield of 57–93 % through the Suzuki coupling reaction of indene-based aryl boronic esters with the commercially available formyl aryl halides (see Support Information for the details). To our delight, all the substrates worked well under this condensation reaction condition promoted by *t*-BuOK, providing the corresponding azulene-embedded PAHs (**1b**–**1m**) in consistently excellent yields (up to 96 %, Table 1). It is noteworthy that the substrates with the heterocyclic ring in the Ar^2 part were also compatible under the current conditions, offering the furan- and thiophene-fused azulene-embedded products (**1c** and **1d**) in 92 % and 86 % yield, respectively. Notably, the precursors containing the thiophene ring in the Ar^1 part were demonstrated to be more efficient for the condensation reaction, no matter whether the Ar^2 part has either electron-donating (−OMe and -dioxole group) or electron-withdrawing groups ($-CF_3$ and −F), providing the corresponding azulene-embedded PAHs with relatively higher yields from 82 % to 96 % (**1f**–**1k**). Furthermore, the present method was highlighted by the introduction of two heterocycles in Ar^1 and Ar^2 parts to prepare the heteroatom-rich azulene-embedded PAHs (**1l** and **1m**) in 85 % and 94 % yields, respectively. The successful synthesis of thiophene-fused azulene-embedded PAHs provides the possibility for further functionalization and application as organic electronic materials.

Considering the high efficiency of the above condensation reactions under mild and simple basic conditions, we envisioned that a cascade reaction of Suzuki coupling / Knoevenagel-type condensation in one pot would be possible through a suitable catalyst and base system. In this respect, we were pleased to find that 2-dodecylbenzo-[1,2]azuleno[4,5-*b*:7,6-*b*′]dithiophene (**1m**) possessing the thiophene units both in Ar^1 and Ar^2 parts was achieved in 21 % yield together with **2m** (71 % yield) from the starting materials **3m** and **4m** in one pot under the Suzuki reaction condition in the presence of 1.25 equivalent of K_2CO_3 (Scheme 1). Interestingly, the yield of **1m** could be improved to 62 % when increasing the amount of K_2CO_3 to 6.0 equivalent. This straightforward one-pot process provides an operationally simple and economically friendly way to prepare thiophene-rich azulene-embedded PAHs that remains rare in previous reports.

Encouraged by the efficient synthesis of the above non-alternant PAHs with one azulene unit, we further explored the feasibility of this synthetic strategy for constructing larger PAHs containing two azulene units with different structural topologies (**1n**–**1t** in Table 2). Precursors **2n** and **2o** were prepared from the same indene-based intermediate with different aldehydes, which successfully provided two

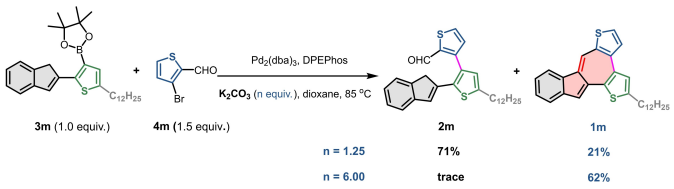

Scheme 1. One-pot synthesis of azulene-embedded PAH **1m**.

Table 2: Synthesis of non-alternant PAHs containing two azulene units.[a]

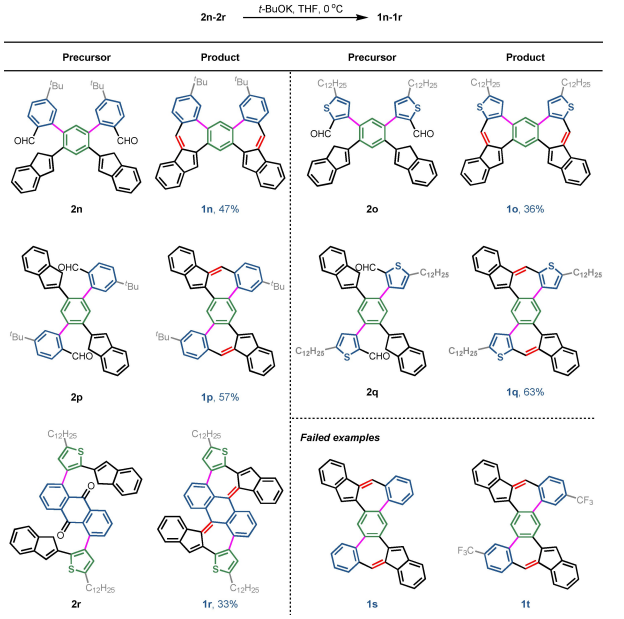

[a] Reaction conditions: **2** (1.0 equiv), *t*-BuOK (3.0 equiv) at 0 °C for 30 min.

benzo- or thiophene-fused butterfly-shaped PAHs, light-red solid **1n** and green solid **1o**, via two-fold Knoevenagel-type condensation reaction in 47 % and 36 % yields, respectively. Furthermore, another two azulene-embedded PAHs with the Z-shape topology (**1p** and **1q**) were prepared by using a similar approach with higher yields of 57 % and 63 %, respectively. We found that in the condensation reaction step the installation of bulky *n*-dodecyl ($C_{12}H_{25}$) or *tert*-butyl groups on the molecular periphery might promote the cyclization process because the synthesis of both **1s** with no substituents and **1t** with trifluoromethyl (CF_3) groups resulted in the decomposed side products (see Supporting Information, Figure S4). Notably, this strategy also provides a practical synthetic approach for the construction of azulene-embedded helicenes. For example, the two-fold condensation reaction of diquinone precursor **2r** gave azulene-embedded double [5]helicene **1r** as a dark-brown solid in 33 % yield, which represents the first double heterohelicene containing two azulene subunits. Therefore, our method revealed a controllable process for constructing fused pentagon-heptagon pairs in large PAHs from easily prepared precursors that are difficult to access by current other methodologies.

The chemical structures of three representative azulene-embedded PAHs **1k**, **1p**, and **1q** were revealed by the X-ray crystallographic analysis,[19] and the optimized structure of double [5]helicene **1r** was also provided for comparison (Figure 2). The thiophene-fused PAHs **1k** and **1q** have a nearly planar backbone with very small dihedral angles ranging from 0.03° to 4.17° in the bay regions (Figures 2a and c). In contrast, benzo-fused compound **1p** displays a twisted geometry with large torsional angles of 13.38° to

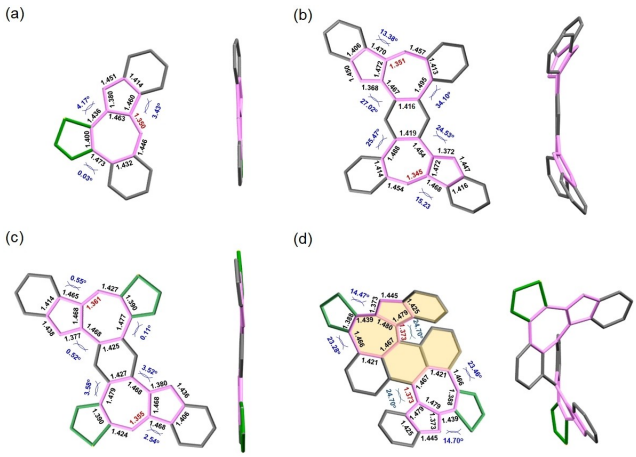

Figure 2. X-ray crystallographic structures of a) **1k**, b) **1p**, c) **1q** as well as the optimized structure of d) **1r** ((*M*, *M*)-isomer is presented here). Alkyl substituents and H atoms are omitted for clarity (azulene unit and thiophene ring are colored in pink and green, respectively, for better visualization; one azulene-embedded [5]helicene unit in **1r** is highlighted with light yellow color).

34.10°, resulting from the large steric repulsion occurring between the hydrogen atoms in the bay positions (Figures 2b). In addition, compounds **1k** and **1q** exhibit weak π–π interaction on account of the long *n*-dodecyl side chain, while compound **1p** shows a close packing distance of 3.68 Å (Figure S6). The azulene-embedded double [5]helicene **1r** possesses a significantly distorted helical structure (Figure 2d) and gives a mean value (24.70°) of three torsional angles for the inner rim of [5]helicene unit, which is larger than that of the pristine [5]helicene (22.63°) and the azulene-embedded [5]helicene (17.73°).[2e,20] DFT calculation displayed that the racemate isomer (*M*, *M*) of **1r** is thermodynamically more stable than its isomer (*P*, *M*) by 11.5 kcal mol^{-1} in terms of Gibbs free energy (Figure S31). Besides, the interconversion between (*M*, *M*) and (*P*, *M*) was proposed to occur through a transition state with the face-to-face terminal benzene rings, of which the isomerization barrier is computed to be 32.4 kcal mol^{-1} at 300 K that is quite larger than the pristine [5]helicene (24.4 kcal mol^{-1}) and the azulene-embedded [5]helicene (12.78 kcal mol^{-1}).[2e,20] Moreover, the above four non-alternant PAHs have similar bond length alternation in the inner azulene unit, where the double bond formed by Knoevenagel-type condensation reaction gives the shortest bond length (1.350 Å for **1k**, 1.345 Å for **1p**, 1.355 Å for **1q** and 1.373 Å for **1r**, respectively) that are slightly longer than those in typical olefins (1.33–1.34 Å). These observations indicate that the new C=C bond generated by condensation still possesses an olefinic double bond feature, which could provide the possible reaction site for further functionalization.

The UV/Vis absorption spectra of the as-synthesized non-alternant PAHs (**1a**–**1r**) were recorded in anhydrous chloroform ($CHCl_3$) to understand their structure and optoelectronic property relationship (Figure 3). For the azulene-embedded PAHs with two benzene rings in both Ar^1 and Ar^2 parts (**1a**, **1b**, **1e**), their UV/Vis spectra exhibited intensive absorption in the range of 300–410 nm with a broad absorption maximized at 449 nm (Figure 3a). Compounds **1d** with the furan ring and **1e** with the thiophene ring in the Ar^2 part showed a significant red-shift of the broad longest-wavelength absorption with the maxima at 489 nm and 501 nm, respectively, which could be attributed to the electron-rich nature of the furan and thiophene rings. In addition, the PAHs with thiophene ring (**1f**–**1k**) in the Ar^1 part exhibited almost similar absorption spectra to that of **1e** (Figure 3b). Notably, **1l** and **1m**, containing two heterocyclic rings both for the Ar^1 and Ar^2 parts, gave a slight red shift of the longest-wavelength absorption maxima in comparison to their mono-heterocycle-embedded counterparts, which may cause by the characteristic n-π* transitions or charge transfer process based on the orbital analysis during the excited states and solvent-dependent absorption spectra (Figure S16). Therefore, the measured optical energy gaps for **1a**–**1m** range from 2.2 eV (**1a**) to 1.76 eV (**1m**). The broad absorption bands of these compounds are well reproduced by TD-DFT calculations, in which the lowest-energy broad absorption bands are attributed to the $S_0 \rightarrow S_1$ transition with small oscillator strength (Figures S17–26). In contrast, the molar extinction coefficient of the PAHs with two azulene units (**1n**–**1r**) is slightly stronger than that of one-azulene-embedded PAHs mentioned above because of the extended

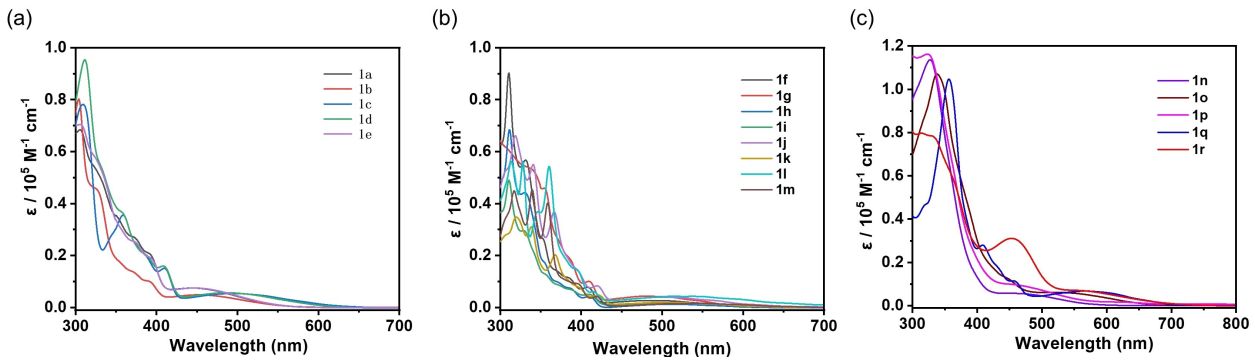

Figure 3. UV/Vis absorption spectra of **1a**–**1e** (a), **1f**–**1m** (b), and **1n**–**1r** (c) were recorded in 1.0×10^{-5} M $CHCl_3$.

π-conjugation (Figure 3c). The longest-wavelength absorption of **1n**–**1r** was observed, ranging from 497 to 455 nm, while their absorption onset was found to range from 597 to 714 nm, giving the corresponding optical energy gaps of 2.07 eV to 1.73 eV. It is noteworthy that double [5]helicene **1r** exhibits intensive absorption around 460 nm, which is quite different from other PAHs in this system. Furthermore, the obtained azulene-embedded PAHs exhibited negligible emission under 365 nm irradiation owing to the intrinsic anti-Kasha behavior of the embedded azulene unit. Normally, azulene-embedded PAHs demonstrate an anti-Kasha emission feature, in which the fluorescence is prone to emit from the S_2 or higher states to the ground state (S_0). However, the obtained azulene-embedded PAHs exhibited negligible emission under 365 nm irradiation. To identify the anti-Kasha emission feature for our azulene-embedded PAHs, TD-DFT calculations for the emission transitions based on the selected compounds (**1a**, **1c**, **1d**, **1n**, **1o**, and **1r**) were performed and discussed in detail. As depicted in Table S13–18, the calculation results suggest that the $S_1 \rightarrow S_0$ transition of the azulene-embedded PAHs is weak (the oscillator strength $f < 0.2$). Especially for **1c**, **1d**, and **1r**, the $S_1 \rightarrow S_0$ transition is nearly forbidden ($f < 0.1$), indicating the possible anti-Kasha emission feature.[21] This phenomenon is similar to other reported ones in azulene-based derivatives.[2c,h] The electrochemical behavior of the selected compounds (**1k**, **1m**, **1q**, and **1r**) was also investigated by CV measurement in degassed and dry CH_2Cl_2 (Figure S7). The one-azulene-embedded compounds **1k** and **1m** exhibited pseudo-reversible and one irreversible oxidation waves with half-wave potentials at 0.16 V/0.28 V and 0.28 V/0.62 V (vs. Fc/Fc^+), respectively. And compounds **1q** and **1r**, possessing two azulene units, displayed two pseudo-reversible oxidation waves with half-wave potentials at 0.18 V/0.79 V and 0.42 V/0.76 V (vs. Fc/Fc^+), respectively. The experiment HOMO levels were estimated to be −4.89, −4.84, −4.90, and −5.05 V for **1k**, **1m**, **1q**, and **1r**, respectively, based on the onset potentials of the first oxidation waves. Accordingly, their experiment LUMO levels are calculated to be −2.91, −3.08, −3.15, and −3.32 V, respectively, based on the corresponding optical energy gaps.

To gain more insights into the local aromaticity of the obtained azulene-embedded PAHs, the nucleus-independent chemical shift (NICS) and the anisotropy of the induced current density (ACID) for all the obtained compounds **1a**–**1r** were calculated.[22] Accordingly, the $NICS(1)_{zz\text{-}avg}$ values for all obtained compounds reveal that the five-membered and seven-membered rings in most compounds demonstrate opposite values, indicating their aromatic or weak aromatic/antiaromatic characters, respectively (Figure S27). As shown in Figure 4a, the $NICS(1)_{zz\text{-}avg}$ values of **1k** were calculated to be −20.3 (ring A), −11.7 (ring B), −11.3 (ring C), −2.9 (ring D) and −16.3 ppm (ring E), respectively, suggesting that the central seven-membered ring has weaker aromaticity than its peripheral rings. Interestingly, the $NICS(1)_{zz\text{-}avg}$ values of the seven-membered rings in **1p** and **1q** became positive around 2.3 to 4.1 ppm (Figure 4b and c), revealing their weak anti-aromaticity mostly resulted from the diatropicity of the surrounding aromatic rings. For **1r**, the $NICS(1)_{zz\text{-}avg}$ value of seven-membered rings is −0.5 ppm for ring B and 2.2 ppm for ring J, respectively, which might be induced by the asymmetric feature of the double helicene units (Figure 4d). In addition, the $NICS(1)_{zz\text{-}avg}$ values of the five-membered rings in **1r** are −1.1 (ring C) and −6.8 (ring I), respectively, indicating their weak aromaticity. In contrast to the central aromatic benzene rings in **1p** (−20.5 ppm, ring E) and **1q** (−18.4 ppm, ring E), the central benzene ring in **1r** is significantly different with a $NICS(1)_{zz\text{-}avg}$ value of 3.0 ppm (ring F), and this could be rationalized by the strong diatropicity effect of its adjacent two benzene rings. The above-calculated aromaticities coincided well with the alternant bond length analysis of **1r**, which can be explained by its highly distorted backbone. Furthermore, the NICS data of all the PAHs is further validated by ACID calculations. Based on the ACID results, the clock-wise diatropic current flow is on the five-membered rings while the counter-clockwise paratropic ring current is on the seven-membered rings (Figure 4 and Figure S29).

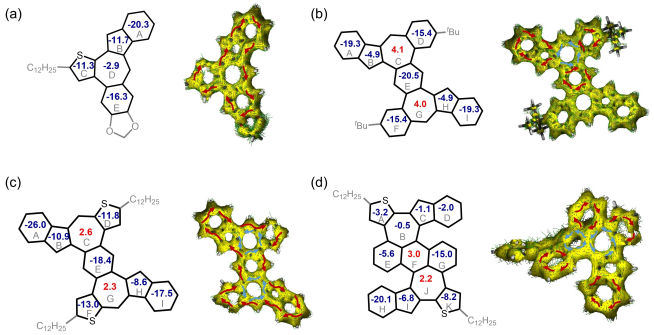

Figure 4. DFT calculated NICS(1)zz-avg values and ACID plots of **1k** (a), **1p** (b), **1q** (c) and **1r** (d) at the GIAO-B3LYP/6-31+G(2d,p) and B3LYP/6-31G(p) level, respectively. Alkyl substituents in the ACID Figures are omitted for clarity.

Conclusion

In conclusion, we presented the synthesis of a new family of azulene-embedded PAHs (**1a**–**1r**) through a simple and efficient synthetic strategy, involving the Suzuki coupling and subsequent Knoevenagel-type condensation starting from the corresponding easily accessible precursors. The condensation process features simplicity scalability, and modularity as well as good-to-excellent reaction yield. The wide variety of the obtained non-alternant PAHs, including the azulene-embedded thiophene-rich PAHs and the first case of two-azulene-embedded double [5]helicene, enabled us to understand the relationship between their structural topology, aromaticity, and photophysical properties. Importantly, we found that the thiophene rings fused to the azulene core can significantly impact the reactivity of the condensation reaction and improve the stability of the large non-alternant PAHs as well as extend their π-conjugations. Further studies on the application of this strategy for the construction of novel non-alternant nanographenes with

contiguous azulene units and azulene-based graphene nanoribbons are currently ongoing in our laboratory.

Acknowledgements

This research was financially supported by the EU Graphene Flagship (Graphene Core 3, 881603), ERC Consolidator Grant (T2DCP, 819698), H2020-MSCA-ITN (ULTIMATE, No. 813036), the Center for Advancing Electronics Dresden (cfaed), H2020-EU.1.2.2.—FET Proactive Grant (LIGHT-CAP, 101017821) and the DFG-SNSF Joint Switzerland-German Research Project (EnhanTopo, No. 429265950). Diffraction data have been collected on BL14.2 at the BESSY II electron storage ring operated by the Helmholtz-Zentrum Berlin; we acknowledge the help of Manfred Weiss and his group members during the experiments at BESSY II. The authors gratefully acknowledge the GWK support for funding this project by providing computing time through the Center for Information Services and HPC (ZIH) at TU Dresden. Open Access funding enabled and organized by Projekt DEAL.

Conflict of Interest

The authors declare no conflict of interest.

Data Availability Statement

The data that support the findings of this study are available from the corresponding author upon reasonable request.

Keywords: Aromaticity · Azulene · Helicenes · Polycyclic Aromatic Hydrocarbons · Structure Elucidation

[1] a) H. Miyoshi, S. Nobusue, A. Shimizu, Y. Tobe, *Chem. Soc. Rev.* **2015**, *44*, 6560–6577; b) Y. Tobe, *Chem. Rec.* **2015**, *15*, 86–96; c) Chaolumen, I. A. Stepek, K. E. Yamada, H. Ito, K. Itami, *Angew. Chem. Int. Ed.* **2021**, *60*, 23508–23532; d) A. Konishi, M. Yasuda, *Chem. Lett.* **2021**, *50*, 195–212; e) Y. Fei, J. Liu, *Adv. Sci.* **2022**, *9*, 2201000.

[2] a) H. Xin, B. Hou, X. Gao, *Acc. Chem. Res.* **2021**, *54*, 1737–1753; b) H. Xin, X. Gao, *ChemPlusChem* **2017**, *82*, 945–956; c) A. Ong, T. Tao, Q. Jiang, Y. Han, Y. Ou, K. Huang, C. Chi, *Angew. Chem. Int. Ed.* **2022**, *61*, e202209286; d) M. Murai, M. Abe, S. Ogi, S. Yamaguchi, *J. Am. Chem. Soc.* **2022**, *144*, 20385–20393; e) C. Duan, J. Zhang, J. Xiang, X. Yang, X. Gao, *Angew. Chem. Int. Ed.* **2022**, *61*, e202201494; f) Q. Jiang, T. Tao, H. Phan, Y. Han, T. Y. Gopalakrishna, T. S. Herng, G. Li, L. Yuan, J. Ding, C. Chi, *Angew. Chem. Int. Ed.* **2018**, *57*, 16737–16741; g) X. Zhang, Y. Huang, J. Zhang, W. Meng, Q. Peng, R. Kong, Z. Xiao, J. Liu, M. Huang, Y. Yi, L. Chen, Q. Fan, G. Lin, Z. Liu, G. Zhang, L. Jiang, D. Zhang, *Angew. Chem. Int. Ed.* **2020**, *59*, 3529–3533; h) S. Wang, M. Tang, L. Wu, L. Bian, L. Jiang, J. Liu, Z.-B. Tang, Y. Liang, Z. Liu, *Angew. Chem. Int. Ed.* **2022**, *61*, e202205658.

[3] a) E. H. K. Ziegler, K. Hafner, *Angew. Chem.* **1955**, *67*, 301–301; b) H. Langhals, M. A. Eberspaecher, *Synthesis* **2018**, *50*, 1862–1866; c) Yu. N. Porshnev, V. B. Mochalin, M. I. Cherkashin, *Russ. Chem. Rev.* **1982**, *51*, 1897–1934.

[4] T. Nozoe, S. Seto, S. Matsumura, Y. Murase, *Bull. Chem. Soc. Jpn.* **1962**, *35*, 1179–1188.

[5] T. Shoji, S. Ito, M. Yasunami, *Int. J. Mol. Sci.* **2021**, *22*, 10686.

[6] a) L. C. Dunn, Y. M. Chang, K. N. Houk, *J. Am. Chem. Soc.* **1976**, *98*, 7095–7096; b) S. E. Reiter, L. C. Dunn, K. N. Houk, *J. Am. Chem. Soc.* **1977**, *99*, 4199–4201.

[7] a) X. Shi, A. Sasmal, J. F. Soulé, H. Doucet, *Chem. Asian J.* **2018**, *13*, 143–157; b) A. H. M. Elwahy, I. A. Abdelhamid, M. R. Shaaban, *ChemistrySelect* **2021**, *6*, 13664–13723; c) Y. Sasaki, M. Takase, T. Okujima, S. Mori, H. Uno, *Org. Lett.* **2019**, *21*, 1900–1903; d) M. Murai, S. Iba, H. Ota, K. Takai, *Org. Lett.* **2017**, *19*, 5585–5588; e) B. Pigulski, K. Shoyama, F. Würthner, *Angew. Chem. Int. Ed.* **2020**, *59*, 15908–15912; f) H. Xin, J. Li, R. Q. Lu, X. Gao, T. M. Swager, *J. Am. Chem. Soc.* **2020**, *142*, 13598–13605; g) Chaolumen, H. Ito, K. Itami, *Chem. Commun.* **2019**, *55*, 9606–9609; h) T. Koide, M. Takesue, T. Murafuji, K. Satomi, Y. Suzuki, J. Kawamata, K. Terai, M. Suzuki, H. Yamada, Y. Shiota, K. Yoshizawa, F. Tani, *ChemPlusChem* **2017**, *82*, 1010–1014; i) K. Uehara, P. Mei, T. Murayama, F. Tani, H. Hayashi, M. Suzuki, N. Aratani, H. Yamada, *Eur. J. Org. Chem.* **2018**, 4508–4511; j) J. Wang, F. Gordillo, J. M. Beloqui, A. Diaz-Andres, X. Miao, D. Casanova, J. Casado, J. Liu, *Angew. Chem. Int. Ed.* **2023**, *62*, e202217124.

[8] a) S. Mishra, T. G. Lohr, C. A. Pignedoli, J. Liu, R. Berger, J. I. Urgel, K. Müllen, X. Feng, P. Ruffieux, R. Fasel, *ACS Nano* **2018**, *12*, 11917–11927; b) T. G. Lohr, J. I. Urgel, K. Eimre, J. Liu, M. Di Giovannantonio, S. Mishra, R. Berger, P. Ruffieux, C. A. Pignedoli, R. Fasel, X. Feng, *J. Am. Chem. Soc.* **2020**, *142*, 13565–13572; c) A. Shiotari, T. Nakae, K. Iwata, S. Mori, T. Okujima, H. Uno, H. Sakaguchi, Y. Sugimoto, *Nat. Commun.* **2017**, *8*, 16089; d) J. Hieulle, E. Carbonell-Sanromà, M. Vilas-Varela, A. Garcia-Lekue, E. Guitián, D. Peña, J. Pascual, *Nano Lett.* **2018**, *18*, 418–423; e) Q. Fan, D. Martin-Jimenez, D. Ebeling, C. K. Krug, L. Brechmann, C. Kohlmeyer, G. Hilt, W. Hieringer, A. Schirmeisen, J. M. Gottfried, *J. Am. Chem. Soc.* **2019**, *141*, 17713–17720.

[9] a) J. Ma, Y. Fu, E. Dmitrieva, F. Liu, H. Komber, F. Hennersdorf, A. A. Popov, J. J. Weigand, J. Liu, X. Feng, *Angew. Chem. Int. Ed.* **2020**, *59*, 5637–5642; b) X. Yang, F. Rominger, M. Mastalerz, *Angew. Chem. Int. Ed.* **2019**, *58*, 17577–17582; c) Y. Han, Z. Xue, G. Li, Y. Gu, Y. Ni, S. Dong, C. Chi, *Angew. Chem. Int. Ed.* **2020**, *59*, 9026–9031; d) L. Yang, Y.-Y. Ju, M. A. Medel, Y. Fu, H. Komber, E. Dmitrieva, J.-J. Zhang, S. Obermann, A. G. Campaña, J. Ma, X. Feng, *Angew. Chem. Int. Ed.* **2023**, *62*, e202216193.

[10] a) J. Liu, S. Mishra, C. A. Pignedoli, D. Passerone, J. I. Urgel, A. Fabrizio, T. G. Lohr, J. Ma, H. Komber, M. Baumgarten, C. Corminboeuf, R. Berger, P. Ruffieux, K. Müllen, R. Fasel, X. Feng, *J. Am. Chem. Soc.* **2019**, *141*, 12011–12020; b) F. Wu, J. Ma, F. Lombardi, Y. Fu, F. Liu, Z. Huang, R. Liu, H. Komber, D. I. Alexandropoulos, E. Dmitrieva, T. G. Lohr, N. Israel, A. A. Popov, J. Liu, L. Bogani, X. Feng, *Angew. Chem. Int. Ed.* **2022**, *61*, e202202170.

[11] a) D. Hibi, K. Kitabayashi, K. Fujita, T. Takeda, Y. Tobe, *J. Org. Chem.* **2016**, *81*, 3735–3743; b) A. Konishi, A. Morinaga, M. Yasuda, *Chem. Eur. J.* **2018**, *24*, 8548–8552; c) K. Yamamoto, M. Okazumi, H. Suemune, K. Usui, *Org. Lett.* **2013**, *15*, 1806–1809; d) F. Zhou, W. Shi, X. Liao, Y. Yang, Z. Yu, J. You, *ACS Catal.* **2022**, *12*, 676–686; e) V. Claus, M. Schukin, S. Harrer, M. Rudolph, F. Rominger, A. M. Asiri, J. Xie, A. S. K. Hashmi, *Angew. Chem. Int. Ed.* **2018**, *57*, 12966–12970.

[12] a) C. Zhu, K. Shoyama, F. Würthner, *Angew. Chem. Int. Ed.* **2020**, *59*, 21505–21509; b) M. Schnitzlein, C. Mützel, K. Shoyama, J. M. Farrell, F. Würthner, *Eur. J. Org. Chem.* **2022**,

e202101273; c) M. Schnitzlein, C. Zhu, K. Shoyama, F. Würthner, *Chem. Eur. J.* **2022**, *28*, e202202053.
[13] N. Ogawa, Y. Yamaoka, H. Takikawa, K. Yamada, K. Takasu, *J. Am. Chem. Soc.* **2020**, *142*, 13322–13327.
[14] a) M. Grzybowski, K. Skonieczny, H. Butenschçn, D. T. Gryko, *Angew. Chem. Int. Ed.* **2013**, *52*, 9900–9930; b) M. Grzybowski, B. Sadowski, H. Butenschön, D. T. Gryko, *Angew. Chem. Int. Ed.* **2020**, *59*, 2998–3027; c) N. Ponugoti, V. Parthasarathy, *Chem. Eur. J.* **2022**, *28*, e202103530; d) Y. Zhang, S. H. Pun, Q. Miao, *Chem. Rev.* **2022**, *122*, 14554–14593.
[15] a) M. S. Mirzaei, A. A. Taherpour, C. Wentrup, *J. Org. Chem.* **2022**, *87*, 3296–3310; b) M. S. Mirzaei, A. A. Taherpour, C. Wentrup, *J. Org. Chem.* **2022**, *87*, 11503–11518.
[16] a) G. Zhang, F. Rominger, U. Zschieschang, H. Klauk, M. Mastalerz, *Chem. Eur. J.* **2016**, *22*, 14840–14845; b) X. Yang, F. Rominger, M. Mastalerz, *Angew. Chem. Int. Ed.* **2021**, *60*, 7941–7946; c) X. Yang, S. M. Elbert, F. Rominger, M. Mastalerz, *J. Am. Chem. Soc.* **2022**, *144*, 9883–9892; d) T. Kirschbaum, F. Rominger, M. Mastalerz, *Angew. Chem. Int. Ed.* **2020**, *59*, 270–274.
[17] M. T. Unruh, U. Scherf, H. Bahmann, A. C. B. Rodrigues, C. Cunha, J. S. Seixas de Melo, J. Schedlbauerd, J. M. Lupton, *J. Mater. Chem. C* **2021**, *9*, 16208–16216.
[18] a) X. Zhuang, W. Zhao, F. Zhang, Y. Cao, F. Liu, S. Bi, X. Feng, *Polym. Chem.* **2016**, *7*, 4176–4181; b) S. Xu, G. Wang, B. P. Biswal, M. Addicoat, S. Paasch, W. Sheng, X. Zhuang, E. Brunner, T. Heine, R. Berger, X. Feng, *Angew. Chem. Int. Ed.* **2019**, *58*, 849–853; c) S. Xu, M. Richter, X. Feng, *Acc. Mater. Res.* **2021**, *2*, 252–265.
[19] Deposition Numbers 2224417, 2224413, and 2224420 contain the supplementary crystallographic data for this paper. These data are provided free of charge by the joint Cambridge Crystallographic Data Centre and Fachinformationszentrum Karlsruhe Access Structures service.
[20] P. Ravat, R. Hinkelmann, D. Steinebrunner, A. Prescimone, I. Bodoky, M. Juríček, *Org. Lett.* **2017**, *19*, 3707–3710.
[21] a) T. Itoh, *Chem. Rev.* **2012**, *112*, 8, 4541–4568; b) X. Chen, D. Tan, J. Dong, T. Ma, Y. Duan, D. Yang, *J. Phys. Chem. Lett.* **2022**, *13*, 43, 10085–10091; c) C. Chen, M. Wang, X. Zhao, S. Yang, X. Chen, X. Wang, *Angew. Chem. Int. Ed.* **2022**, *61*, e202200779.
[22] a) P. R. Schleyer, C. Maerker, A. Dransfeld, H. Jiao, N. J. R. Van Eikema Hommes, *J. Am. Chem. Soc.* **1996**, *118*, 6317–6318; b) Z. Chen, C. S. Wannere, C. Corminboeuf, R. Puchta, P. v. R. Schleyer, *Chem. Rev.* **2005**, *105*, 3842–3888; c) D. Geuenich, K. Hess, F. Köhler, R. Herges, *Chem. Rev.* **2005**, *105*, 3758–3772.

Manuscript received: December 25, 2022
Accepted manuscript online: March 6, 2023
Version of record online: April 17, 2023